Title: Brg1 controls stemness and metastasis of pancreatic cancer through regulating hypoxia pathway

Authors: Osamu Araki[1], Motoyuki Tsuda[1], Mayuki Omatsu[1], Mio Namikawa[1], Makoto Sono[1], Yuichi Fukunaga[1,2], Tomonori Masuda[1], Takaaki Yoshikawa[1], Munemasa Nagao[1], Satoshi Ogawa[1], Kenji Masuo[1], Norihiro Goto[1], Yu Muta[1], Yukiko Hiramatsu[1], Takahisa Maruno[1], Yuki Nakanishi[1], Sho Koyasu[3], Toshihiko Masui[4], Etsuro Hatano[4], Dieter Saur[5], Akihisa Fukuda[1], Hiroshi Seno[1]

Affiliations:

[1] Department of Gastroenterology and Hepatology, Kyoto University Graduate School of Medicine, Kyoto, Japan

[2] Department of Drug Discovery Medicine, Medical Innovation Center, Kyoto University Graduate School of Medicine, Kyoto, Japan

[3] Departments of Diagnostic Imaging and Nuclear Medicine, Kyoto University Graduate School of Medicine, Kyoto, Japan

[4] Division of Hepato-Biliary-Pancreatic Surgery and Transplantation, Department of Surgery, Kyoto University Graduate School of Medicine, Kyoto, Japan

[5] Department of Internal Medicine II, Klinikum rechts der Isar, Technische Universität München, München, Germany.

Corresponding author:

Akihisa Fukuda MD, PhD

Department of Gastroenterology and Hepatology, Kyoto University Graduate School of Medicine, 54 Shogoin-Kawahara-cho, Sakyo-ku, Kyoto, 606-8507, Japan.

E-mail: fukuda26@kuhp.kyoto-u.ac.jp

Phone: +81-75-751-4319

Fax: +81-75-753-4303

Competing interests:

This author discloses the following: Yuichi Fukunaga is employed by Sumitomo Dainippon Pharma. The remaining authors disclose no conflicts.

Abstract

Pancreatic ductal adenocarcinoma (PDAC) is a devastating disease. We previously reported that chromatin remodeler Brg1 is essential for acinar cell-derived PDAC formation in mice. However, the functional role of Brg1 in established PDAC and its metastasis remains unknown. Here, we investigated the importance of Brg1 for established PDAC by using a mouse model with a dual recombinase system. We discovered that Brg1 was a critical player for the cell survival and growth of spontaneously developed PDAC in mice. Additionally, Brg1 was essential for metastasis of PDAC cells by inhibiting apoptosis in splenic injection and peritoneal dissemination models. Moreover, cancer stem-like property was compromised in PDAC cells by Brg1 ablation. Mechanistically, the hypoxia pathway was downregulated in Brg1-deleted mouse PDAC and BRG1-low human PDAC. Brg1 was essential for HIF-1α to bind to its target genes to augment the hypoxia pathway, which was important for PDAC cells to maintain their stem-like properties and to metastasize to the liver. Human PDAC cells with high BRG1 expression were more susceptible to BRG1 suppression. In conclusion, Brg1 plays a critical role for cell survival, stem-like property and metastasis of PDAC through the regulation of hypoxia pathway, and thus could be a novel therapeutic target for PDAC.

Introduction

Pancreatic ductal adenocarcinoma (PDAC) is the fourth leading cause of cancer-related mortality. Despite many efforts to develop effective therapies over several decades, the 5-year survival of PDAC patients is approximately 10%, and even worse in patients with distant metastases. Thus, there is an urgent need for new therapeutic approaches to treat this lethal disease. To this end, it is crucial to identify the decisive factors that control PDAC initiation and progression and to understand the underlying molecular mechanisms.

ATP-dependent chromatin remodeling complexes are a group of epigenetic regulators that control gene expression by altering the chromatin structure making it more accessible to DNA binding factors using energy generated by hydrolyzing ATP[1, 2]. SWI/SNF complex is a major family of ATP-dependent chromatin remodeling complexes. Approximately 14% of human PDAC have mutations in genes encoding subunits of SWI/SNF complex, which are considered to be one of the ten major categories of PDAC mutations[3]. *BRG1*, also known as *SMARCA4*, encodes a catalytic ATPase subunit of the SWI/SNF complex. It is mutated in only a few percent of human PDAC but is inactivated in approximately 10-20% of human PDAC specimens[4, 5]. Whether BRG1 functions as a tumor driver or as a tumor suppressor depends on tumor types. BRG1 is frequently absent and/or mutated in several cancer types[4], suggesting that it has a tumor suppressive role. Other studies have shown that BRG1 is necessary for cancer cell proliferation in several cancer types[6-8]. In terms of PDAC, BRG1 expression has been shown to be significantly correlated with higher-stage and higher-tumor grade[9], which is in conflict with another report of a worse prognosis for patients with BRG1-deficient PDAC[10]. We previously showed that pancreatic intraepithelial neoplasia (PanIN), which is pancreatic precancerous lesion, required Brg1 for its formation and also for its maintenance to avoid apoptosis[5]. However, the function of Brg1 in the progression of established PDAC is still unknown.

In PDAC, as well as in other cancer types, stemness promotes each step of metastasis, from primary tumor to a distant organ. This includes migration from primary lesion and intravasation[11], as well as colonization and tumor initiation in distant organs[12]. Brg1 supports the maintenance of the stemness in several cancer types as well as in normal tissue[13-15]. However, the role of Brg1 in cancer metastasis is controversial[16, 17] and its importance in stemness and metastasis has not been thoroughly explored in PDAC.

Therefore, in this study, we sought to clarify the function of Brg1 in established PDAC derived from PanIN and metastasis, as well as to determine whether Brg1 may be a therapeutic target for invasive PDAC.

Results

Brg1 plays an important role in growth of spontaneously developed invasive PDAC in mice.

To assess the BRG1 expression in PDAC, we performed immunohistochemistry for Brg1 on PDAC specimens of mouse and human. We found that the BRG1 expression of most PDAC cells was higher than that of normal acinar cells in both mouse and human (Supplementary Fig. 1). To determine the effect of Brg1 knockout (KO) on established invasive PDAC *in vivo*, we used a genetically engineered mouse model taking advantage of a novel dual recombinase system[18]. We crossed *Pdx1-Flp; Kras*$^{FSF\text{-}G12D/+}$*; Trp53*$^{frt/+}$*; Rosa26*$^{FSF\text{-}CreERT2}$ mice with *Brg1*$^{lox/lox}$ mice to generate *Pdx1-Flp; Kras*$^{FSF\text{-}G12D/+}$*; Trp53*$^{frt/+}$*; Rosa26*$^{FSF\text{-}CreERT2}$*; Brg1*$^{lox/lox}$ (*BKPFC*) mice (Fig. 1A). In this model, Flp-frt recombinase system induced expression of mutant *Kras*^{G12D} allele, *Trp53* heterozygous allele, and tamoxifen-inducible *Cre*^{ERT2} allele in the pancreatic epithelium, which led to the development of spontaneous PDAC derived from PanIN. Administration of tamoxifen allowed us to inactivate Brg1 by utilizing the Cre-loxP system after PDAC was established.

We first assessed the effect of Brg1 ablation on the growth of PDAC tumor by ultrasound scan analysis using this spontaneously developed PDAC mouse model (Fig. 1B); *Pdx1-Flp; Kras*$^{FSF\text{-}G12D/+}$*; Trp53*$^{frt/+}$*; Brg1*$^{lox/lox}$ (*BKPF*) mice as control group and *BKPFC* mice as Brg1 KO group. Since the knockout efficiency of Brg1 after one-week tamoxifen administration was varied for each PDAC tumor, we included to the analysis the tumors of Brg1 KO group in which more than fifty percent of PDAC cells were Brg1-negative for histological evaluation (Fig. 1C). Comparison of the size of PDACs between before and after the tamoxifen administration showed that the growth rate of the PDAC tumors in Brg1 KO group was significantly smaller than that in control group (Fig. 1D, E).

Proliferation and apoptosis in Brg1 KO cells in established PDAC were analyzed by

immunohistochemistry (Fig. 1F-I). There were significantly fewer Ki67-positive proliferative PDAC cells (Fig. 1F, G) and more cleaved caspase 3 (CC3)-positive apoptotic PDAC cells (Fig. 1H, I) in Brg1 KO tumors than in controls. These results indicated that Brg1 loss impacted the maintenance of spontaneously developed invasive PDAC in mice through suppressing both proliferation and survival of PDAC cells.

Brg1 is essential for cell proliferation and survival of PDAC cells *in vitro*.

To further investigate the effect of the Brg1 ablation on PDAC cells, we established PDAC cell lines from PDAC tumors developed in *BKPFC* mice and ablated Brg1 by administrating 4-hydroxytamoxifen (4-OHT) *in vitro* (Fig. 2A). Brg1 expression was almost completely absent at both the RNA (Fig. 2B) and protein (Fig. 2C) levels. Cell viability assays showed that Brg1 loss markedly suppressed the growth of PDAC cells *in vitro* (Fig. 2D, E). Cell cycle analysis showed that Brg1 ablation significantly reduced the number of S phase PDAC cells (Fig. 2F, G), indicating that the cell cycle was inhibited. Annexin V assays revealed that Brg1 loss significantly affected the viability of PDAC cells (Fig. 2H).

The effect of Brg1 ablation on the growth of murine PDAC cells was measured by using a subcutaneous transplantation model (Fig. 2I). Consistent with the data from the spontaneously developed PDAC mouse model and the *in vitro* model, Brg1 loss restricted the PDAC cell growth in the subcutaneous transplantation model (Fig. 2J, K). Histology revealed significantly fewer Ki67-positive proliferative cells (Fig. 2L, N) and significantly more CC3-positive apoptotic cells in Brg1-ablated PDAC cells than in control PDAC cells (Fig. 2M, N). Collectively, Brg1 is essential for both cell proliferation and survival of mouse PDAC cells through regulation of the cell cycle and inhibition of apoptosis *in vitro* and *in vivo.*

Brg1 plays an essential role in metastasis of mouse PDAC cells through inhibiting

apoptosis.

We next investigated the role of Brg1 for the metastatic potential of mouse PDAC cells by utilizing an intrasplenic injection model (Fig. 3A). Macroscopically, numerous liver metastases were formed in mice transplanted with control PDAC cells at 14 days after intrasplenic injection, whereas liver metastases were rarely formed in mice transplanted with Brg1 KO PDAC cells (Fig. 3B, C). Immunostaining revealed a dramatically reduced number of CK19 positive metastatic sites in the liver of mice transplanted with Brg1 KO PDAC cells compared with control PDAC cells (Fig. 3D, E). Notably, almost all the rare liver metastatic lesions formed in mice injected with Brg1 KO PDAC cells were composed of Brg1-positive PDAC cells (Fig. 3F, G), indicating these lesions derived from Brg1-positive “escaper” cells. These data suggested that Brg1 plays an essential role in liver metastasis of mouse PDAC cells *in vivo*.

We next investigated kinetics of Brg1 KO PDAC cells in the liver after splenic injection by tracing the luciferase signal transfected to cancer cells. Bioluminescence imaging analysis revealed that control PDAC cells expanded continually in the liver after the splenic injection, whereas Brg1 KO PDAC cells increased until day 4, then gradually decreased, and finally disappeared around 6 to 8 days after the injection (Fig. 3H, I). Histological analysis showed that significantly increased numbers of apoptotic cells were present in Brg1 KO group than in control group 4 days after transplantation (Fig. 3J, K). These results showed that Brg1 KO PDAC cells initially colonize the liver parenchyma, then gradually decrease and eventually disappear due to apoptosis.

To further investigate the importance of Brg1 in advanced stage of tumorigenesis, we transplanted Brg1 KO PDAC cells into the abdominal cavities of C57BL/6 mice to mimic peritoneal dissemination (Supplementary Fig. 2A). Numbers of peritoneal dissemination were observed in mice transplanted with control PDAC cells, whereas peritoneal dissemination

was not formed in mice transplanted with Brg1 KO PDAC cells (Supplementary Fig. 2B). Bioluminescence imaging confirmed peritoneal dissemination in mice transplanted with control PDAC cells, whereas Brg1 KO PDAC cells did not expand and eventually disappeared (Supplementary Fig. 2C, D). Thus, Brg1 is also essential for peritoneal dissemination of mouse PDAC cells *in vivo.*

These results further strengthen the conclusion that Brg1 is required for distant metastasis of mouse PDAC cells through inhibiting apoptosis *in vivo.*

Brg1 regulates stem-like properties of PDAC cells.

Given the potential importance of cancer stem cells in metastasis[12], we tested if cancer stemness property is compromised in Brg1 KO PDAC cells. Expression of the stem cell markers such a *Aldh1a1*, *Epcam*, *Nes*, and *Jag1* was significantly downregulated in Brg1 KO PDAC cells compared to those in control PDAC cells (Fig. 4A). Sphere formation assays in three-dimensional (3D) conditions showed that Brg1 KO PDAC cells formed significantly fewer spheres than control PDAC cells both in Matrigel (Fig. 4B) and soft agar (Fig. 4C, D). In addition, evaluation of apoptosis in a suspension culture, which was known to be enriched with cancer stem cells, compared to in an adherent culture (Fig. 4E, F) showed that significantly increased apoptosis was observed in Brg1 KO PDAC cells compared to control PDAC cells in both culture conditions, although a more prominent difference was seen in suspension culture (Fig. 4G, H). Thus, these results indicated that Brg1 regulates cancer stem-like property of mouse PDAC cells and suggested that loss of cancer stem-like property by Brg1 ablation results in apoptotic cell death and compromised metastatic potentials of PDAC cells in mice.

Brg1 has a tumor promotive role in PDAC cells in the context of Trp53 null condition.

In the lung cancer, previous reports showed that loss of Brg1 concurrently with Trp53 loss increases tumor burden and shortens survival [19]. We next investigated whether loss of Brg1 in the context of homozygous *Trp53* loss might give a different phenotype from that in the heterozygous *Trp53* loss background. To this end, we generated *Pdx1-Flp; Kras*$^{FSF\text{-}G12D/+}$*; Trp53*$^{frt/frt}$*; Rosa26*$^{FSF\text{-}CreERT2}$*; Brg1*$^{lox/lox}$ (*BKP*^{homo}*FC*) mice and established a PDAC cell line from a PDAC tumor developed in *BKP*^{homo}*FC* mice. After confirming that *Brg1* was efficiently knocked out with 4-OHT treatment in those PDAC cells (Supplementary Fig. 3A), we found that PDAC cells with *Trp53* homozygous deletion represented exactly the same phenotype as those with *Trp53* heterozygous deletion, as determined by cell viability assay, subcutaneous transplantation experiments, sphere formation assay, and intrasplenic transplantation experiments (Supplementary Fig. 3B-G). Furthermore, we next evaluated the Trp53 status of PDAC cells from both *BKPFC* and *BKP*^{homo}*FC* mice and found that *Trp53* wild type allele was deleted in all three different PDAC cell lines from *BKPFC* mice (Supplementary Fig. 3H) and that there was no *Trp53* expression in all *BKPFC* PDAC cells, as determined by qRT-PCR analysis (Supplementary Fig. 3I). Therefore, Brg1 has a tumor promotive role in PDAC cells in the context of Trp53 null condition as well.

Brg1 ablation downregulates metabolic pathway, cell cycle, and stemness genes.

To provide insights into the molecular mechanism, we performed unbiased transcriptomic analysis of Brg1 KO PDAC cells. The gene expression patterns were analogous among three different Brg1 KO *BKPFC* PDAC samples (Fig. 5A). Five hundred and seventy-three and 629 genes were upregulated and downregulated in Brg1 KO PDAC cells relative to control PDAC cells, respectively (Fig. 5B). Gene-set enrichment analysis (GSEA) revealed that there were much more hallmark gene sets significantly downregulated than upregulated in Brg1 KO PDAC cells compared with control PDAC cells with only the INTERFERON ALFA

RESPONSE gene set upregulated (Fig. 5C). Meanwhile, downregulated hallmark gene sets in Brg1 KO PDAC cells included those associated with the cell cycle (G2M_CHECKPOINT, E2F_TARGETS) and metabolic pathways (CHOLESTEROL_HOMEOSTASIS, HYPOXIA, GLYCOLYSIS). This was consistent with our previous result that Brg1 regulates cell-cycle progression. Moreover, among the curated gene sets, gene sets related to embryonic stem cells were significantly downregulated in Brg1 KO PDAC cells, consistent with the findings that the stem-like property was impaired in Brg1 KO PDAC cells (Fig. 5D).

Brg1 and Brm function as mutually exclusive catalytic subunits of the SWI/SNF complex. To examine whether there was compensatory upregulation of *Brm* in response to Brg1 deletion, we investigated the expression of the other SWI/SNF subunits in Brg1 KO PDAC cells by using microarray data (Supplementary Fig. 4A). The expression of *Brm* was not increased in Brg1 KO PDAC cells compared to control PDAC cells, indicating that compensatory upregulation of *Brm* did not occur in Brg1 KO PDAC cells. On the other hand, the expression of other SWI/SNF subunits, such as *Arid1b* and *Arid2*, was upregulated in Brg1 KO PDAC cells compared to control PDAC cells, suggesting the possibility that compensatory upregulation of these subunits was observed in Brg1 KO PDAC cells.

Brg1 functions as a chromatin opener and directly regulates expression of genes including HIF-1 signaling pathway.

Transcriptomic data contained the genes which were regulated by Brg1 both directly and indirectly. To identify the genes that Brg1 directly regulates, we performed ChIP-seq analysis of Brg1, H3K27ac as an open chromatin marker, and H3K27me3 as a closed chromatin marker. Most genes with Brg1 peaks had Brg1-H3K27ac overlapped peaks (Fig. 5E), consistent with previous reports showing that the SWI/SNF complex functions as a chromatin opener[20]. In accordance with this context, few Brg1 peaks overlapped with the H3K27me3

peaks (Supplementary Fig. 5A). Some of the H3K27ac peaks were significantly decreased by Brg1 KO ("H3K27ac down" peaks) and more than half of the genes with "H3K27ac down" peaks were overlapped with the genes which had Brg1 peaks (Fig. 5E), indicating that Brg1 directly regulated their chromatin states. In contrast, none of H3K27me3 peaks were altered by Brg1 KO, further supporting the notion that the SWI/SNF complex functions as a chromatin opener.

Next, we analyzed the distribution of the peaks over genomic regions. By comparing the distribution of Brg1 binding regions with that of Brg1- "H3K27ac down" overlapping regions, we found that Brg1 directly regulated the chromatin state rather in intergenic regions such as enhancers than in promoters (Supplementary Fig. 5B). Motif analysis revealed that each AP-1 component was enriched in Brg1-binding sites and no apparent difference was seen in Brg1 directly regulating sites (Supplementary Fig. 5C, D). These results are consistent with the previous study showing that AP-1 binds to enhancers with SWI/SNF complex[21].

To determine the genes that Brg1 directly regulates in PDAC cells, we integrated ChIP-seq and microarray data to search for genes that had Brg1- "H3K27ac down" overlapping peaks and were downregulated by Brg1 KO in the same PDAC cells and identified 797 genes (Fig. 5F). Pathway analysis of these genes identified the potential pathways that Brg1 directly regulates, including HIF-1 signaling pathway and metabolic pathway (Fig. 5G).

Brg1 directly regulates expression of HIF target genes in PDAC cells.

Given the transcriptomic and ChIP-seq data, we focused on the hypoxia pathway, because it was commonly seen in the results of both analyses ("hypoxia" in GSEA of microarray data, "HIF-1 signaling pathway" in pathway analysis of Brg1 directly regulated genes). Expression of HIF target genes such as *Bnip3*, *Vegfa*, *Trf*, and *Bcl2l1*, was upregulated in the detached condition in control PDAC cells, which was in agreement with

the previous report[22] (Fig. 6A, B). In Brg1 KO PDAC cells, the expression of those HIF target genes was significantly reduced in both the attached and detached conditions compared to controls. These results suggested that Brg1 regulates the hypoxia pathway, which is upregulated in stem cells.

On the other hand, there were no differences in HIF-1α expression between control and Brg1 KO PDAC cells at both the mRNA and protein levels. To investigate the discrepancy of the expression change between HIF-1α and its target genes, we examined HIF-1α binding to its regulatory elements. According to the ChIP-seq data, Brg1- “H3K27ac down” overlapping peaks were enriched with the hypoxia responsive element (HRE) motif (Fig. 6C), which was considered to be the HIF binding site, suggesting that Brg1 is involved in HIF binding to the HRE sites of HIF target genes. ChIP assay for HIF-1α in several HRE sites showed that HIF-1α binding to the HRE sites of target genes was significantly reduced in Brg1 KO PDAC cells compared to controls (Fig. 6D), indicating that Brg1 facilitates HIF-1α binding to the HRE sites of HIF target genes in order to directly regulate their expression.

Histological analysis of liver metastases 4 days after the splenic injection, when Brg1 KO PDAC cells started to disappear, showed that HIF-1α was expressed in both control and Brg1 KO PDAC cells, but in contrast, the expression of HIF target genes, including Bnip3 and Bcl-xL, was downregulated in Brg1 KO PDAC cells (Fig. 6E). These IHC results further confirmed our *in vitro* findings described above (Fig. 6A, B).

Collectively, these data demonstrated that Brg1 regulates HIF-1α binding to the HRE sites of HIF target genes in order to directly regulate their expression in PDAC cells in mice.

Brg1 plays a critical role in cell survival, stem-like property, and metastasis of PDAC cells through regulating the hypoxia pathway.

We hypothesized that Brg1 promotes proliferation, cancer stem-like property, and metastasis of PDAC cells through activating the hypoxia pathway. To test this hypothesis, we next evaluated the effect of suppressing the hypoxia pathway on cell proliferation, cancer stem-like property, and metastasis of PDAC cells by silencing *Hif1a.* We introduced shHif1a into the mouse PDAC cells described above (Fig. 6F). No significant difference in proliferation was observed between *Hif1a*-silenced PDAC cells and controls (Fig. 6G). In contrast, the sphere-forming ability of PDAC cells was significantly attenuated in *Hif1a*-silenced PDAC cells compared to controls (Fig. 6H, I). Moreover, intrasplenic injection experiments revealed significant reduction of liver metastases in *Hif1a* silenced PDAC cells compared to controls (Fig. 6J-M). These results indicated that cancer stem-like property and metastasis are impaired by *Hif1a* suppression.

Collectively, we concluded that Brg1 plays a critical role for cancer stem-like property and metastasis of PDAC cells, at least in part, through regulating the hypoxia pathway.

Expression level of BRG1 correlates with the tumor-suppressive effect of BRG1 suppression on proliferation and stem-like property in human PDAC cells.

The human PDAC transcriptomic data from the Cancer Genome Atlas (TCGA) database were used to compare the specimens with low and high BRG1 expression. In good agreement with the mouse data, GSEA showed that the similar gene sets were downregulated in human PDAC with low BRG1 expression compared to high BRG1 expression, including gene sets associated with cell cycle, metabolic pathways, stemness, and hypoxia pathway (Fig. 7A-C), supporting the notion that BRG1 is important for augmenting the hypoxia pathway in human PDAC.

The effect of BRG1 suppression on proliferation and stem-like property in human PDAC cells was investigated using nine human PDAC cell lines with BRG1 suppression by an RNA

interference method using pooled siRNA (Supplementary Fig. 6A). Proliferation and stem-like property were impaired by BRG1 suppression in multiple human PDAC cell lines (Fig. 7D, E), consistent with the mouse data. To further confirm this finding, we ablated *BRG1* in MIAPaCa-2, AsPC-1, and Panc-1 cells using the CRISPR/Cas9-encoding adenovirus and found that *BRG1* ablation suppressed proliferation and stem-like property in those cells, as was observed in *BRG1* knockdown (Supplementary Fig. 6B, C). Further, the degree of proliferation and stem-like property inhibition by BRG1 suppression differed among them (Fig. 7F, G). To determine whether these differences were correlated with the protein expression levels of BRG1 and HIF-1α in each PDAC cell, we examined these protein expressions of each PDAC cell (Fig. 7H, I).

Initially, Panc-1, Capan-2, and KP4 cells had no observable BRG1 protein expression by western blotting, with only minor expression of BRG1 mRNA (Fig. 7J), consistent with a previous report[23]. However, we demonstrated BRG1 protein expression in those PDAC cells by immunoblotting using a highly sensitive substrate (Supplementary Fig. 6D). Furthermore, in order to validate on-target activity of siRNAs, we performed the same experiments by using three different single siRNAs on Panc-1 and Capan-2 (Supplementary Fig. 6E) and obtained the same results as those using pooled siRNAs. In addition, the expression of possible off-target genes of those single siRNAs was not changed by administration of those siRNAs in Panc-1 and Capan-2 cells, as determined by q-PCR analysis (Supplementary Fig. 7). We also confirmed that *BRG1* overexpression rescued the effect of BRG1 suppression on viability and sphere formation in Panc-1 and KP4 cells (Supplementary Fig. 6F-I). BRG1 ablation by CRISPR/Cas9 also suppressed the growth of Panc-1 cells (Supplementary Fig. 6B, C). We validated the frequencies of off-target effect of adenoviruses bearing sgRNA against BRG1 by sequencing the region downstream of the target sequences or possible off-target sites and found that off-target effect was extremely

low (Supplementary Fig. 8). The level of BRG1 expression significantly correlated with the inhibitory effect of BRG1 suppression on proliferation and sphere formation in human PDAC cells, whereas that was not the case with HIF-1α expression (Fig. 7K, L). The inhibitory effect of BRG1 suppression did not appear to be related to the mutations of the major tumor suppressor genes, including *CDKN2A*, *TRP53*, and *SMAD4*. (Supplementary Fig. 6J).

In good agreements with our mouse data, BRG1 suppression inhibits proliferation and stem-like property of human PDAC cells and expression levels of BRG1 are correlated with the tumor suppressive effect of BRG1 suppression on proliferation and stem-like property in human PDAC cells.

Discussion

In this study, to clarify the functions of Brg1 in established PDAC, we developed a genetically engineered mouse model using a dual recombinase system, which enabled us to inactivate Brg1 upon tamoxifen administration after PDAC developed *in vivo*. We established PDAC cells from these mouse tumors and evaluated the role of Brg1 in proliferation and metastasis by deleting Brg1, both *in vitro* and *in vivo*. We demonstrated for the first time that Brg1 regulates the cell survival and growth of spontaneously developed PDAC and metastasis through the control of the cancer stem-like property of PDAC cells in mice. These data indicate that Brg1 is a promising therapeutic target for PDAC.

In this study, we found that Brg1 plays a critical role for progression of established PDAC derived from acinar cell-originated PanIN. Regarding PDAC initiation, our previous report showed that Brg1 is essential for formation of acinar cell-originated PanIN and PanIN-derived PDAC, which was mediated by direct regulation of Sox9 by Brg1[5]. As for duct cell-derived PDAC, Brg1 suppresses formation of duct cell-originated IPMN and IPMN-derived PDAC[10]. Thus, cell of origin is a critical factor that determines the role of Brg1 in PDAC initiation. In contrast, regarding progression of established PDAC, another report showed that Brg1 has a tumor-promoting effect in duct cell-originating IPMN-derived PDAC by supporting a mesenchymal-like transcriptional landscape[24]. Brg1 re-expression into duct cell-originating IPMN-derived Brg1 null PDAC cells increased anchorage-independent cell growth and proliferation, indicating that Brg1 re-expression into Brg1 null PDAC cells enhances tumorigenicity[24]. In this current study, we showed that Brg1 plays a tumor promoting role for established PanIN-derived PDAC. Furthermore, the current study for the first time revealed that Brg1 is essential for metastasis of PDAC cells, which was, mediated, at least in part, by direct regulation of the hypoxia pathway by Brg1.Therefore, our data together with the previous reports demonstrate that BRG1 plays a tumor-promotive role for progression of

established PDAC regardless of its cellular origin and premalignant lesion. These data highlight cell type-specific and context-dependent roles of Brg1 in PDAC initiation and progression at different stages.

We demonstrated that Brg1 is essential for metastasis of PDAC cells by using splenic injection and intraperitoneal dissemination models. Furthermore, we showed that the mechanistic reason why Brg1-negative PDAC cells could only rarely form metastatic lesions was neither because they were disappeared in the blood stream nor because they could not anchor to the liver, but because they could not form metastatic lesions after colonization due to apoptosis. The role of Brg1 in cancer metastasis was ambiguous in previous knockdown studies with one showing that Brg1 is important for gastric cancer metastasis, whereas another showed the opposite in colorectal cancer. These differences may result from different mechanisms in each cancer types, knockdown efficiency of target genes, or from differing periods between transduction of shRNAs and the transplantation into mice. In our knockout model, Brg1 was completely deleted in each PDAC cell and Brg1-negative PDAC cells were established in a short period of time. Thus, we clearly demonstrated that Brg1 is required for cell survival and metastasis of PDAC cells *in vivo*.

We also showed that the cancer stem-like property was compromised in PDAC cells by Brg1 ablation, consistent with the notion that cancer stemness is a critical factor for metastasis. Previous studies have demonstrated the importance of BRG1 on cancer stem-cell maintenance in liver cancer[13, 14] and colon cancer[17]. In the current study, we showed for the first time that Brg1 plays acritical role for the stem-like property of PDAC, as determined by three different sphere formation assays including Matrigel, soft agar sphere formation assays, and suspension culture. In terms of the suspension culture experiment, we cannot completely rule out the possibility that Brg1 ablation might impair the sphere formation by inhibiting cell aggregation, but not by inhibiting stem-like property. However, we concluded

that Brg1 is critical for stem-like property, because cell aggregation did not affect the results of the other two sphere formation assays.

We found that Brg1 activates the hypoxia pathway through supporting HIF-1α binding to the hypoxia responsive elements of HIF target genes based on transcriptomic and ChIP analyses of mouse PDAC cells. We discovered that the hypoxia pathway is a mediator of Brg1 in mouse PDAC and that *Hif1a* silencing partially phenocopied mouse Brg1 KO PDAC cells. Increased expression of HIF-1α or HIF-2α has been reported in many types of cancer including PDAC[25], and the expression of both genes increased in cancer stem cells. Each HIF-α subunit is necessary for cancer stemness in several types of cancer, including PDAC[25, 26]. In this study, *Hif1a* silencing did not produce a complete phenocopy, probably because HIF-2α may play an important role in the proliferation, stemness, and metastasis of mouse PDAC cells. As a limitation of this study, we did not investigate the correlative relationship between the hypoxia pathway and cell viability or inhibition of cell death. Future study is needed to clarify how Brg1 regulates stem-like property and metastasis through the hypoxia pathway in more detail.

We found that Brg1 plays an important role in PDAC growth by supporting cell-cycle progression and cell survival in both *in vivo* and *in vitro* experiments. Previous studies showed that BRG1 is involved in proliferation in association with TOPIIa[27, 28], cell-cycle related genes[29, 30], and phosphoinositide-3-kinase-protein kinase B/AKT (PI3K/AKT) pathway[31-33] by *in vitro* studies. In this work, the precise mechanism of Brg1 regulation of cell-cycle progression was unclear, however, transcriptomic analysis suggested that the MYC pathway could be a mediator, since it has long been known to be associated with proliferation; moreover, gene sets of MYC targets were downregulated both in Brg1 KO mouse PDAC cells and in human PDAC samples with low Brg1 expression.

We showed that BRG1 expression was positively correlated with the hypoxia pathway and that BRG1 was also essential for proliferation and stem-like property of both human PDAC and mouse PDAC cells. Given that Brg1 is expressed in around 80% of human PDAC[5] , we have provided novel and significant insights that suggest therapeutic approaches. Moreover, the expression levels of BRG1was significantly correlated with the inhibitory effect of BRG1 suppression on proliferation and stem-like property in human PDAC cells. Future study is needed to determine if the BRG1 is an effective therapeutic target in BRG1-expressing human PDAC, as well as whether the expression level of BRG1 provide suitable biomarkers for BRG1-targeted therapy.

The role of SWI/SNF complex in cancer is context dependent and each subunit functions differently. As for BRG1, as described above, Brg1 has an opposite function in PDAC initiation and progression depending on its stage and cell type: Brg1 inhibits formation of duct cell-originated IPMN-derived PDAC initiation, whereas Brg1 plays a critical role for PDAC progression. In lung cancer and cancer of unknown primary site, BRG1 loss is associated with poor prognosis for survival in non-small cell lung cancer, indicating that BRG1 has a tumor-suppressive role in these cancer types[34]. In contrast, BRG1 suppression reduces proliferation in other cancer types[6-8] . These findings underscore the context-dependent role of BRG1 in cancer depending on cancer cell types. The role of BRM, a mutually exclusive subunit of BRG1, also differs between cancer types. Loss of BRM leads to worse prognosis in lung cancer[35], which is opposite of pancreatic cancer[9]. BRM suppression reduces proliferation in several cancer types[36, 37]. ARID1A, the most mutated subunit in the SWI/SNF complex in cancer, also has a context-dependent role in several cancer types. In PDAC, we previously reported that Arid1a suppresses duct cell-originated IPMN-derived PDAC formation similarly to Brg1[38]. Other group showed that Arid1a also suppresses PanIN-derived PDAC formation[39, 40], which is the opposite function to Brg1 in terms of

initiation of PanIN-derived PDAC. Arid1a also has the context-dependent roles in hepatocellular carcinoma[41]. Arid1a promotes initiation of hepatocellular carcinoma, whereas its loss promoted progression and metastasis of liver tumors. Collectively, the function of subunits of the SWI/SNF complex in cancer differs depending on cancer cell types, stage of carcinogenesis. Thus, targeting SWI/SNF complex for cancer therapy may be complicated.

For developing therapy targeting BRG1, investigation of its effect on the normal tissues cannot be avoided. Brg1 is dispensable for pancreatic development[10], however, we previously showed that Brg1 is essential for intestinal stem cells and intestinal crypt-villous formation[42]. BRG1 is also required for hematopoietic stem cells and neural stem cells[43] as well as liver regeneration[44]. Therefore, BRG1 inhibition can affect the normal tissues. Careful assessment of the effect of BRG1 inhibition on normal tissues is needed for developing therapy targeting BRG1.

In conclusion, we demonstrated that Brg1 plays a crucial role for cell survival and growth of spontaneously developed PDAC. We also showed that Brg1 is essential for metastasis and the cancer stem-like property of PDAC cells in mice partially by regulating HIF-1α binding to the hypoxia responsive elements of HIF-1α target genes to directly regulate their expression. Therefore, BRG1 may be a novel therapeutic target for PDAC.

Materials & Methods

Detailed methods are described in Supplementary Materials and Methods. Primer sequences are described in Supplementary Table 1, 2, 3, and 4. Primer antibodies are listed in Supplementary Table 5.

Mice.

The following strains were used: *Brg1*^{lox} (a gift from David Reisman, University of Florida, Gainesville, Florida, USA, with permission from Pierre Chambon, University of Strasbourg Institute for Advanced Study, Strasbourg, France)[45], *Pdx1-Flp*, *Kras*$^{FSF\text{-}G12D}$, and *R26*$^{FSF\text{-}CreERT2}$ [18]. Mice were crossed in a mixed background, with no selection for a specific sex. Tamoxifen (Sigma-Aldrich, St. Louis, MO) was dissolved in corn oil (20 mg/ml) and administered intraperitoneally, with each mouse receiving 2 mg in each injection. All animal experiments were approved by the animal research committee of Kyoto University and performed in accordance with Japanese government regulations.

RNA isolation and quantitative real-time PCR (qRT-PCR) analysis.

RNA was isolated using the RNeasy Kit (QIAGEN, Venlo, Nederland). Complementary DNA was synthesized using the ReverTra Ace qPCR RT Kit (Toyobo, Osaka, Japan). Quantitative PCR (qPCR) was performed with a SYBR Green–based gene-expression assay using a LightCycler 96 System (Roche, Basel, Switzerland). Expression levels were normalized using *Actb* (mouse) or *ACTB* (human) as a reference gene. Primer sequences for the analyzed genes are listed in Supplementary Tables 2 and 3. All reactions were performed in duplicate or triplicate.

Histology and immunostaining.

Mouse tissue was fixed in 4% w/v paraformaldehyde in PBS for 2 days at 4°C, dehydrated into 70% v/v ethanol, embedded in paraffin, and cut into 5 μm thick sections. Paraffin-embedded sections were deparaffinized, rehydrated, and stained with hematoxylin and eosin (H&E) or used for immunostaining. For immunostaining, sections were incubated with 3% v/v H_2O_2 for 10 min to quench endogenous peroxidases, incubated with citric acid buffer (pH 6.0) or EDTA buffer (pH 8.0) for 15 min at 98°C for antigen retrieval, and blocked using blocking solution (Dako) for 30 minutes at RT. Incubation with primary antibodies were either overnight at 4°C or for 2 h at RT. Secondary antibody incubation was for 1 h at RT using biotinylated secondary antibody (Vector Laboratories, Burlingame, CA). Slides were developed using the VECTASTAIN ABC Kit (Vector Laboratories) and Liquid DAB+ Substrate Chromogen System (Dako), followed by counterstaining with hematoxylin. For immunofluorescence staining, antigen retrieval, blocking, and primary antibody incubation were performed as described above. Sections were then incubated with fluorescence-conjugated secondary antibody (Thermo Fisher Scientific, Waltham, MA) for 1 h at RT, followed by staining with Hoechst solution to visualize nuclei.

Dilutions of primary antibody are listed in Supplementary Table 5.

Cytokeratin 19 (CK19) positive areas were measured using Image J software (NIH Image).

Human PDACs specimens.

Surgically resected specimens of human pancreatic cancer tissues were obtained from patients who had been admitted to Kyoto University Hospital. The study protocol (#G1200-1, R2904) was approved by the Ethics Committee of Kyoto University Hospital.

Statistical analysis.

In vitro and *in vivo* data are presented as means ± standard errors of the mean (SEM).

All statistical analyses were performed using either GraphPad Prism (version 6.0) or Microsoft Excel 2016.

Acknowledgements

The authors thank all members of the Fukuda laboratory for technical assistance and helpful discussions. This work was supported in part by Grants-in-Aid KAKENHI (19H03639, 19K16712, 19K22619, 20H03659). It was also supported by Japan Agency for Medical Research and Development, the Project for Cancer Research and Therapeutic Evolution (18cm0106142h0001, 20cm0106177h0001, 20cm0106375h0001) and AMED-PRIME (20gm6010022h0003), Moonshot Research and Development Program (JPMJMS2022-1), and COI-NEXT (JPMJPF2018). It was also supported by Princess Takamatsu Cancer Research Fund (17-24924), the Mochida Foundation (2017bvAg), the Mitsubishi Foundation (201910037), the Uehara Foundation (201720143), the Naito Foundation (22205-1), the Kobayashi Foundation (203200700019), the Simizu Foundation (203180700103), the Japan Foundation for Applied Enzymology (203190700054), the SGH Foundation (203200700056), the Kanae Foundation (203190700083), the Bristol Myers Squibb (200190700011), the Ichiro Kanehara Foundation (20KI037), and the Takeda Foundation (201749741, 203200700045). A part of this study was conducted through the CORE Program of the Radiation Biology Center, Kyoto University.

Author contributions

OA, MT and AF conceived and designed the study. OA, MT, TY, MN, SO, YH and TM performed the experiments and analyzed the data. MN, MS, YF, TM, MO, KM, YM, NG and SK contributed reagents, materials, and analysis tools. TM and EH contributed surgical specimens. DS generated *Pdx1-Flp, Kras$^{FSF\text{-}G12D}$, Trp53^{frt}, and R26$^{FSF\text{-}CreERT2}$* mice. OA wrote the manuscript and YN, AF, and HS revised it. AF organized the study.

Data availability

All original microarray data were deposited in the Gene Expression Omnibus (GEO) at National Center for Biotechnology Information (NCBI) with series accession no. GSE199442. The complete ChIP-Seq data were deposited in the GEO at NCBI with series accession no. GSE199610.

References

1 Saha A, Wittmeyer J, Cairns BR. Chromatin remodelling: the industrial revolution of DNA around histones. *Nat Rev Mol Cell Biol* 2006; 7: 437-447.

2 Lorch Y, Maier-Davis B, Kornberg RD. Mechanism of chromatin remodeling. *Proc Natl Acad Sci U S A* 2010; 107: 3458-3462.

3 Bailey P, Chang DK, Nones K, Johns AL, Patch AM, Gingras MC *et al.* Genomic analyses identify molecular subtypes of pancreatic cancer. *Nature* 2016; 531: 47-52.

4 Marquez-Vilendrer SB, Thompson K, Lu L, Reisman D. Mechanism of BRG1 silencing in primary cancers. *Oncotarget* 2016; 7: 56153-56169.

5 Tsuda M, Fukuda A, Roy N, Hiramatsu Y, Leonhardt L, Kakiuchi N *et al.* The BRG1/SOX9 axis is critical for acinar cell-derived pancreatic tumorigenesis. *J Clin Invest* 2018; 128: 3475-3489.

6 Wu Q, Madany P, Dobson JR, Schnabl JM, Sharma S, Smith TC *et al.* The BRG1 chromatin remodeling enzyme links cancer cell metabolism and proliferation. *Oncotarget* 2016; 7: 38270-

38281.

7 Shi J, Whyte WA, Zepeda-Mendoza CJ, Milazzo JP, Shen C, Roe JS *et al.* Role of SWI/SNF in acute leukemia maintenance and enhancer-mediated Myc regulation. *Genes Dev* 2013; 27: 2648-2662.

8 Romero OA, Torres-Diz M, Pros E, Savola S, Gomez A, Moran S *et al.* MAX inactivation in small cell lung cancer disrupts MYC-SWI/SNF programs and is synthetic lethal with BRG1. *Cancer Discov* 2014; 4: 292-303.

9 Numata M, Morinaga S, Watanabe T, Tamagawa H, Yamamoto N, Shiozawa M *et al.* The clinical significance of SWI/SNF complex in pancreatic cancer. *Int J Oncol* 2013; 42: 403-410.

10 von Figura G, Fukuda A, Roy N, Liku ME, Morris Iv JP, Kim GE *et al.* The chromatin regulator Brg1 suppresses formation of intraductal papillary mucinous neoplasm and pancreatic ductal adenocarcinoma. *Nat Cell Biol* 2014; 16: 255-267.

11 Hermann PC, Huber SL, Herrler T, Aicher A, Ellwart JW, Guba M *et al.* Distinct populations of cancer stem cells determine tumor growth and metastatic activity in human pancreatic cancer.

Cell Stem Cell 2007; 1: 313-323.

12 Ito H, Tanaka S, Akiyama Y, Shimada S, Adikrisna R, Matsumura S *et al.* Dominant Expression of DCLK1 in Human Pancreatic Cancer Stem Cells Accelerates Tumor Invasion and Metastasis. *PLoS One* 2016; 11: e0146564.

13 Zhu P, Wang Y, Wu J, Huang G, Liu B, Ye B *et al.* LncBRM initiates YAP1 signalling activation to drive self-renewal of liver cancer stem cells. *Nat Commun* 2016; 7: 13608.

14 Shi DM, Shi XL, Xing KL, Zhou HX, Lu LL, Wu WZ. miR-296-5p suppresses stem cell potency of hepatocellular carcinoma cells via regulating Brg1/Sall4 axis. *Cell Signal* 2020; 72: 109650.

15 Yan X, Han D, Chen Z, Han C, Dong W, Han L *et al.* RUNX2 interacts with BRG1 to target CD44 for promoting invasion and migration of colorectal cancer cells. *Cancer Cell Int* 2020; 20: 505.

16 Huang LY, Zhao J, Chen H, Wan L, Inuzuka H, Guo J *et al.* SCF(FBW7)-mediated degradation of Brg1 suppresses gastric cancer metastasis. *Nat Commun* 2018; 9: 3569.

17 Wang G, Fu Y, Yang X, Luo X, Wang J, Gong J *et al*. Brg-1 targeting of novel miR550a-5p/RNF43/Wnt signaling axis regulates colorectal cancer metastasis. *Oncogene* 2016; 35: 651-661.

18 Schönhuber N, Seidler B, Schuck K, Veltkamp C, Schachtler C, Zukowska M *et al*. A next-generation dual-recombinase system for time- and host-specific targeting of pancreatic cancer. *Nat Med* 2014; 20: 1340-1347.

19 Lissanu Deribe Y, Sun Y, Terranova C, Khan F, Martinez-Ledesma J, Gay J *et al*. Mutations in the SWI/SNF complex induce a targetable dependence on oxidative phosphorylation in lung cancer. *Nat Med* 2018; 24: 1047-1057.

20 Schnitzler G, Sif S, Kingston RE. Human SWI/SNF interconverts a nucleosome between its base state and a stable remodeled state. *Cell* 1998; 94: 17-27.

21 Vierbuchen T, Ling E, Cowley CJ, Couch CH, Wang X, Harmin DA *et al*. AP-1 Transcription Factors and the BAF Complex Mediate Signal-Dependent Enhancer Selection. *Mol Cell* 2017; 68: 1067-1082.e1012.

622 22 Labuschagne CF, Cheung EC, Blagih J, Domart MC, Vousden KH. Cell Clustering Promotes a
623 Metabolic Switch that Supports Metastatic Colonization. *Cell Metab* 2019; 30: 720-734.e725.
624
625 23 Shain AH, Giacomini CP, Matsukuma K, Karikari CA, Bashyam MD, Hidalgo M *et al.* Convergent
626 structural alterations define SWItch/Sucrose NonFermentable (SWI/SNF) chromatin remodeler as
627 a central tumor suppressive complex in pancreatic cancer. *Proc Natl Acad Sci U S A* 2012; 109:
628 E252-259.
629
630 24 Roy N, Malik S, Villanueva KE, Urano A, Lu X, Von Figura G *et al.* Brg1 promotes both tumor-
631 suppressive and oncogenic activities at distinct stages of pancreatic cancer formation. *Genes Dev*
632 2015; 29: 658-671.
633
634 25 Zhang Q, Lou Y, Zhang J, Fu Q, Wei T, Sun X *et al.* Hypoxia-inducible factor-2α promotes tumor
635 progression and has crosstalk with Wnt/ß-catenin signaling in pancreatic cancer. *Mol Cancer* 2017;
636 16: 119.
637
638 26 Cao XP, Cao Y, Li WJ, Zhang HH, Zhu ZM. P4HA1/HIF1α feedback loop drives the glycolytic and
639 malignant phenotypes of pancreatic cancer. *Biochem Biophys Res Commun* 2019; 516: 606-612.

27 Bourgo RJ, Siddiqui H, Fox S, Solomon D, Sansam CG, Yaniv M *et al*. SWI/SNF deficiency results in aberrant chromatin organization, mitotic failure, and diminished proliferative capacity. *Mol Biol Cell* 2009; 20: 3192-3199.

28 Dykhuizen EC, Hargreaves DC, Miller EL, Cui K, Korshunov A, Kool M *et al*. BAF complexes facilitate decatenation of DNA by topoisomerase IIα. *Nature* 2013; 497: 624-627.

29 Sobczak M, Pietrzak J, Płoszaj T, Robaszkiewicz A. BRG1 Activates Proliferation and Transcription of Cell Cycle-Dependent Genes in Breast Cancer Cells. *Cancers (Basel)* 2020; 12.

30 Bai J, Mei PJ, Liu H, Li C, Li W, Wu YP *et al*. BRG1 expression is increased in human glioma and controls glioma cell proliferation, migration and invasion in vitro. *J Cancer Res Clin Oncol* 2012; 138: 991-998.

31 Liu X, Tian X, Wang F, Ma Y, Kornmann M, Yang Y. BRG1 promotes chemoresistance of pancreatic cancer cells through crosstalking with Akt signalling. *Eur J Cancer* 2014; 50: 2251-2262.

658 32 Jubierre L, Soriano A, Planells-Ferrer L, París-Coderch L, Tenbaum SP, Romero OA *et al.*
659 BRG1/SMARCA4 is essential for neuroblastoma cell viability through modulation of cell death and
660 survival pathways. *Oncogene* 2016; 35: 5179-5190.
661
662 33 Lv DJ, Song XL, Huang B, Yu YZ, Shu FP, Wang C *et al.* HMGB1 Promotes Prostate Cancer
663 Development and Metastasis by Interacting with Brahma-Related Gene 1 and Activating the Akt
664 Signaling Pathway. *Theranostics* 2019; 9: 5166-5182.
665
666 34 Concepcion CP, Ma S, LaFave LM, Bhutkar A, Liu M, DeAngelo LP *et al.* Smarca4 Inactivation
667 Promotes Lineage-Specific Transformation and Early Metastatic Features in the Lung. *Cancer*
668 *Discov* 2022; 12: 562-585.
669
670 35 Fukuoka J, Fujii T, Shih JH, Dracheva T, Meerzaman D, Player A *et al.* Chromatin remodeling
671 factors and BRM/BRG1 expression as prognostic indicators in non-small cell lung cancer. *Clin*
672 *Cancer Res* 2004; 10: 4314-4324.
673
674 36 Zhang Z, Wang F, Du C, Guo H, Ma L, Liu X *et al.* BRM/SMARCA2 promotes the proliferation and
675 chemoresistance of pancreatic cancer cells by targeting JAK2/STAT3 signaling. *Cancer Lett* 2017;

402: 213-224.

37 Wu Q, Madany P, Akech J, Dobson JR, Douthwright S, Browne G *et al.* The SWI/SNF ATPases Are Required for Triple Negative Breast Cancer Cell Proliferation. *J Cell Physiol* 2015; 230: 2683-2694.

38 Kimura Y, Fukuda A, Ogawa S, Maruno T, Takada Y, Tsuda M *et al.* ARID1A Maintains Differentiation of Pancreatic Ductal Cells and Inhibits Development of Pancreatic Ductal Adenocarcinoma in Mice. *Gastroenterology* 2018; 155: 194-209.e192.

39 Wang W, Friedland SC, Guo B, O'Dell MR, Alexander WB, Whitney-Miller CL *et al.* ARID1A, a SWI/SNF subunit, is critical to acinar cell homeostasis and regeneration and is a barrier to transformation and epithelial-mesenchymal transition in the pancreas. *Gut* 2019; 68: 1245-1258.

40 Wang SC, Nassour I, Xiao S, Zhang S, Luo X, Lee J *et al.* SWI/SNF component ARID1A restrains pancreatic neoplasia formation. *Gut* 2019; 68: 1259-1270.

41 Sun X, Wang SC, Wei Y, Luo X, Jia Y, Li L *et al.* Arid1a Has Context-Dependent Oncogenic and Tumor Suppressor Functions in Liver Cancer. *Cancer Cell* 2017; 32: 574-589.e576.

42 Takada Y, Fukuda A, Chiba T, Seno H. Brg1 plays an essential role in development and homeostasis of the duodenum through regulation of Notch signaling. *Development* 2016; 143: 3532-3539.

43 Güneş C, Paszkowski-Rogacz M, Rahmig S, Khattak S, Camgöz A, Wermke M *et al.* Comparative RNAi Screens in Isogenic Human Stem Cells Reveal SMARCA4 as a Differential Regulator. *Stem Cell Reports* 2019; 12: 1084-1098.

44 Wang B, Kaufmann B, Engleitner T, Lu M, Mogler C, Olsavszky V *et al.* Brg1 promotes liver regeneration after partial hepatectomy via regulation of cell cycle. *Sci Rep* 2019; 9: 2320.

45 Sumi-Ichinose C, Ichinose H, Metzger D, Chambon P. SNF2beta-BRG1 is essential for the viability of F9 murine embryonal carcinoma cells. *Mol Cell Biol* 1997; 17: 5976-5986.

Figure Legends

Figure 1. Brg1 plays an important role in the growth of spontaneously developed invasive PDAC in mice.

(A) Genetic strategy to ablate Brg1 upon tamoxifen administration in established PDAC in *Pdx1-Flp; Kras$^{FSF\text{-}G12D/+}$; Trp53$^{frt/+}$; Rosa26$^{FSF\text{-}CreERT2}$; Brg1$^{lox/lox}$* (*BKPFC* or Brg1 KO) mice.

(B) Experimental design of sonographic analysis and tamoxifen administration. Tamoxifen was administered intraperitoneally (2 mg per mouse) for 7 d.

(C) Percentage of Brg1-positive PDAC cells after one-week tamoxifen administration in *BKPFC* (Brg1 KO) mice. n = 6.

(D) Rate of PDAC volume change analyzed by ultrasound scan in *BKPF* (control) mice (n = 10) and *BKPFC* (Brg1 KO) mice (n = 6) after one-week tamoxifen administration.

(E) Representative sonographic images of PDAC tumors before and after tamoxifen administration.

(F) Fluorescence micrographs of PDAC after one-week tamoxifen administration for Brg1 (green), cytokeratin (CK) (red), Ki67 (white), and the merged image. Scale bar, 100 μm.

(G) Quantification of Ki67-positive PDAC cells in control mice (all PDAC cells were Brg1-positive) (n = 5) and of Brg1-negative PDAC cells in Brg1 KO mice (n = 6).

(H) Representative histology of PDAC after one-week tamoxifen administration stained with haematoxilin and eosin (H&E) and stained to detect cytokeratin 19 (CK19), Brg1, and cleaved-caspase 3 (CC3). Scale bar, 100 μm.

(I) Quantification of CC3-positive cells in PDAC of control (n = 5) and Brg1 KO mice (n = 6).

All data are stated as mean ± SEM. *p < 0.05, Student's *t*-test.

Figure 2. Brg1 is critical for cell proliferation and survival of PDAC cells *in vitro*.

(A) Experimental design of 4-OHT administration preceding assays shown in (B)-(H). 4-OHT

was administered in the Brg1 KO group and methanol (MeOH) was administered in the control (control) group both at 1μM. Scale bar, 100 μm.

(B, C) Efficiency of Brg1 knockout with 4-OHT administration on mRNA levels (B) and protein levels (C).

(D) Representative images of the clonogenic assay. 4-OHT was administered after seeding of PDAC cells onto 6-well plates.

(E) Sequential quantification of PDAC cell viability of control and Brg1 KO groups. 4-OHT was administered day 1 ,2, and 3.

(F, G) Cell cycle analysis with EdU and propidium iodide (PI). Representative images (F) and percentages of EdU-positive S phase PDAC cells (G). n=3.

(H) Percentage of Annexin V-positive PDAC cells. n = 3.

(I) Experimental design for subcutaneous transplantation of PDAC cells and tamoxifen administration. Tamoxifen was administered intraperitoneally 5 d per week 14 d after transplantation.

(J) Subcutaneous tumors on day 25 after transplantation.

(K) Volume of subcutaneous tumors on the indicated days after transplantation.

(L) Quantification of Ki67-positive PDAC cells in the subcutaneous tumors of the control (n = 6) and Brg1 KO (n = 10) groups.

(M) Quantification of CC3-positive PDAC cells in the subcutaneous tumors of the control (n = 6) and Brg1 KO (n = 10) groups.

(N) Representative images of subcutaneous tumors stained with H&E and for Brg1, CK19, Ki67, and CC3. Scale bar, 100 μm.

All data are shown as mean ± SEM. *$p < 0.05$, Student's *t*-test.

Figure 3. Brg1 plays an essential role for liver metastasis of mouse PDAC cells by inhibiting apoptosis *in vivo*.

(A) Experimental design for 4-OHT administration to PDAC cells *in vitro* and intrasplenic injection. 4-OHT and methanol were administered daily for 3 d at 1 μM with splenic injection performed on day 4.

(B) Representative images of liver metastases 14 d after splenic injection.

(C) Percentage of liver weight to body weight 14 d after splenic injection in the control (n = 3) and Brg1 KO (n = 5) groups.

(D) Representative images of CK19 staining of liver metastases.

(E) Percentage of CK19-positive area determined by combining five independent sections together in the control (n = 3) and Brg1 KO (n = 5) groups.

(F) Representative images of liver metastases stained with H&E and immunostained for CK19, Brg1. Scale bar, 100 μm.

(G) Percentage of Brg1-positive PDAC cells in each metastatic lesion in the liver of Brg1 KO group. n = 10.

(H) Representative bioluminescence imaging of PDAC cells in the liver after intrasplenic injection.

(I) Bioluminescence plot of liver metastases at indicated time points after intrasplenic injection in the control (n = 5) and Brg1 KO (n = 4) groups.

(J) Representative images of liver metastases 4 d after intrasplenic injection stained with H&E, and immunostained for Brg1, CK and CC3 in combination with Hoechst 33342 for nuclear staining. Scale bar, 100 μm.

(K) Percentage of CC3-positive cells to CK-positive metastatic PDAC cells.

All data are shown as mean ± SEM. *$p < 0.05$, Student's t test.

Figure 4. Brg1 is critically important for cancer stem-like property of PDAC cells.

(A) Relative mRNA levels of indicated genes related to PDAC stem cells as determined by qRT-PCR in PDAC cells treated with methanol (control) or 4-OHT (Brg1 KO) daily for 3 d. n = 3.

(B) Representative images of Matrigel limiting dilution assays and table showing numbers of sphere-containing wells per 5 wells. PDAC cells were seeded in Matrigel after treated with methanol (control) or 4-OHT (Brg1 KO) daily for 3 d. Scale bar, 200 μm.

(C) Representative images of soft agar colony formation assays. Scale bar, 500 μm.

(D) Quantification of colonies in soft agar colony formation assays. n = 3.

(E) Experimental design for Annexin V analysis on attached (att) and detached (det) conditions. PDAC cells were seeded on adherent culture plates and treated with methanol (control) or 4-OHT (Brg1 KO) daily for 3 d. Cells were analyzed on day 4 for attached condition and passaged to cell-repellent culture plates on day 3 and analyzed on day 4 for detached condition.

(F) Representative images of PDAC cells in suspension culture on day 4. Scale bar, 200 μm.

(G) Annexin V-FITC and ethidium homodimer III assays.

(H) Percentages of Annexin V-positive PDAC cells. n = 3.

All data are shown as mean ± SEM. *p < 0.05, Student's *t*-test.

Figure 5. Brg1 plays a critical role for metastasis and cancer stem-like property of PDAC cells through directly regulating the expression of HIF target genes.

(A) Heatmap visualization of differentially expressed genes with hierarchical clustering analysis.

(B) Volcano plot of transcriptomic data. Genes downregulated in Brg1 KO PDAC cells with fold change < 0.5 and p-value < 0.05 were colored with blue and genes upregulated in Brg1

KO group with fold change > 2.0 and p-value < 0.05 colored with red.

(C) Hallmark gene sets significantly downregulated in Brg1 KO PDAC cells.

(D) Significantly downregulated gene sets associated with stemness in Brg1 KO PDAC cells.

(E) Venn diagram of genes with Brg1 peaks, genes with H3K27ac peaks, and genes with H3K27ac peaks which were significantly reduced when Brg1 was knocked out ("H3K27ac down"). Genes in the intersections of different circles had overlapping regions of both peaks.

(F) Venn diagram of genes with overlapping peaks between Brg1 and "H3K27ac down" and genes whose mRNA expression were downregulated with fold change < 0.7 in Brg1 KO PDAC cells in the transcriptomic data.

(G) Pathway analysis of the genes which is common to both regions shown in (F).

Figure 6. Brg1 directly regulates the expression of HIF target genes in PDAC cells.

(A, B) PDAC cells were treated as indicated in Fig. 4E.

(A) Relative mRNA levels of *Hif1a* and HIF target genes determined by qRT-PCR. n = 3.

(B) Immunoblot for Brg1, HIF-1α, HIF target gene Bnip3, CC3, and β-Actin.

(C) Enrichment of HRE motifs in Brg1 and "H3K27ac down" overlapping lesion based on ChIP-seq data.

(D) ChIP-qPCR of HIF-1α at the representative HRE regions in control and Brg1 KO PDAC cells. Relative fold enrichment of HIF-1α over IgG on the HRE regions of indicated HIF target genes. n = 5.

(E) Representative images of liver metastases 4 d after intrasplenic injection immunostained for Brg1; HIF target genes Bnip3 and Bcl-xL; and HIF-1α. Images stained for Brg1, Bnip3, and Bcl-xL were serial sections in control and Brg1 KO groups, respectively. Arrowheads indicate Brg1-deleted PDAC cells. Scale bar, 100 μm.

(F) Efficiency of *Hif1a* knockdown by shHif1a lentivirus transduction in mouse PDAC cells.

Two different shHif1a constructs were used.

(G) Quantification of PDAC cell viability of control and *Hif1a* knockdown PDAC cells. n = 3.

(H, I) Matrigel sphere formation assay of control and *Hif1a* knockdown PDAC cells. (J) Representative images of spheres. Scale bar, 200 μm. (K) Sphere formation rates. n = 4.

(J-M) Liver metastases after intrasplenic injection of control and *Hif1a* knockdown PDAC cells. (J) Bioluminescence images on day 6. (K) Sequential plot of bioluminescence signal intensities of liver metastases at indicated time points after intrasplenic injection. (L) Representative images of liver metastases on day 8 after intrasplenic injection. (M) Percentage of liver weight to body weight on day 8 after intrasplenic injection in control (n = 4) and *Hif1a* knockdown (shHif1a #1, n = 3; shHif1a #2, n = 3) groups.

All data are shown as mean ± SEM. *p < 0.05, Student's *t*-test.

Figure 7. Brg1 expression is a predictive determinant of BRG1 knockdown efficacy of suppression of human PDAC cell proliferation and stem-like property.

(A) Hallmark gene sets significantly downregulated in human PDAC samples with low Brg1 expression. RNA-seq data obtained from TCGA database and samples with Brg1 expression in the top quartile and bottom quartile were compared by GSEA.

(B) Gene sets associated with stemness significantly downregulated in low Brg1 expression group in GSEA of human PDAC samples.

(C) Gene sets associated with the hypoxia pathway significantly downregulated in low Brg1 expression group in GSEA of human PDAC samples.

(D) Viability of human PDAC cell lines on day 1, 3 and 5 treated with siCtrl or siBRG1 on day 1. MIA PaCa-2, n = 3; BxPC3, CFPAC-1, n = 5; the others, n = 4.

(E) Matrigel sphere formation assays of human PDAC cell lines treated with siCtrl or siBRG1. PDAC cells treated with siRNA for 24 h were embedded in Matrigel and analyzed on day 5.

n = 3.

(F) Relative viability of human PDAC cells treated with siBRG1 compared to siCtrl on day 5 shown in (D).

(G) Relative sphere formation rate of human PDAC cells treated with siBRG1 compared to siCtrl shown in (E).

(H) Immunoblotting of extracts from each human PDAC cell line for BRG1 and HIF-1α.

(I) Relative quantification of the band density of BRG1 and HIF-1α calculated by dividing with the β-Actin from panel (H). n = 3.

(J) Relative mRNA levels of *BRG1* by qRT-PCR in human PDAC cells. n = 3.

(K) Correlation between the relative viability calculated in (F) and BRG1 and HIF-1α protein expression in each human PDAC cell line. Scatter plot represents the correlation between the relative viability and BRG1 protein expression. X-axis represents relative BRG1 expression of each human PDAC cell line to that of BxPC3.

(L) Correlation between the relative sphere forming rate calculated in (G) and BRG1 and HIF-1α protein expression in each human PDAC cell line. Scatter plot represents the correlation between the relative sphere forming rate and BRG1 protein expression. X-axis represents relative BRG1 expression of each human PDAC cell line to that of BxPC3.

All data are shown as mean ± SEM. *$p < 0.05$. Student's *t*-test.

Figure 1

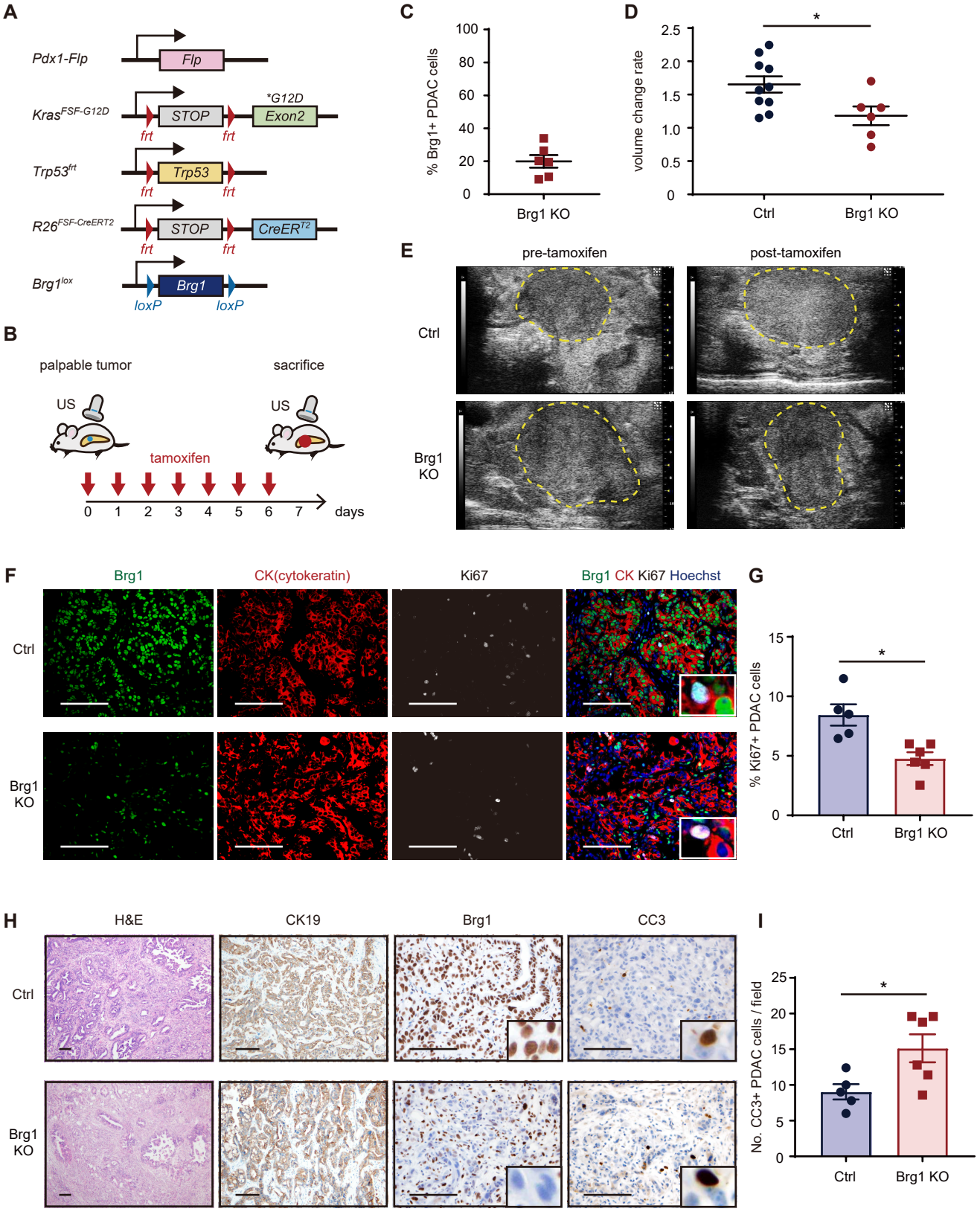
A
Pdx1-Flp
Flp
Kras^FSF-G12D
STOP
*G12D
Exon2
frt
frt
Trp53^frt
Trp53
frt
frt
R26^FSF-CreERT2
STOP
CreER^T2
frt
frt
Brg1^lox
Brg1
loxP
loxP
B
palpable tumor
sacrifice
US
US
tamoxifen
0 1 2 3 4 5 6 7
days
C
% Brg1+ PDAC cells
100
80
60
40
20
0
Brg1 KO
D
volume change rate
2.5
2.0
1.5
1.0
0.5
0
*
Ctrl
Brg1 KO
E
pre-tamoxifen
post-tamoxifen
Ctrl
Brg1 KO
F
Brg1
CK(cytokeratin)
Ki67
Brg1 CK Ki67 Hoechst
Ctrl
Brg1 KO
G
% Ki67+ PDAC cells
15
10
5
0
*
Ctrl
Brg1 KO
H
H&E
CK19
Brg1
CC3
Ctrl
Brg1 KO
I
No. CC3+ PDAC cells / field
25
20
15
10
5
0
*
Ctrl
Brg1 KO

Figure 2

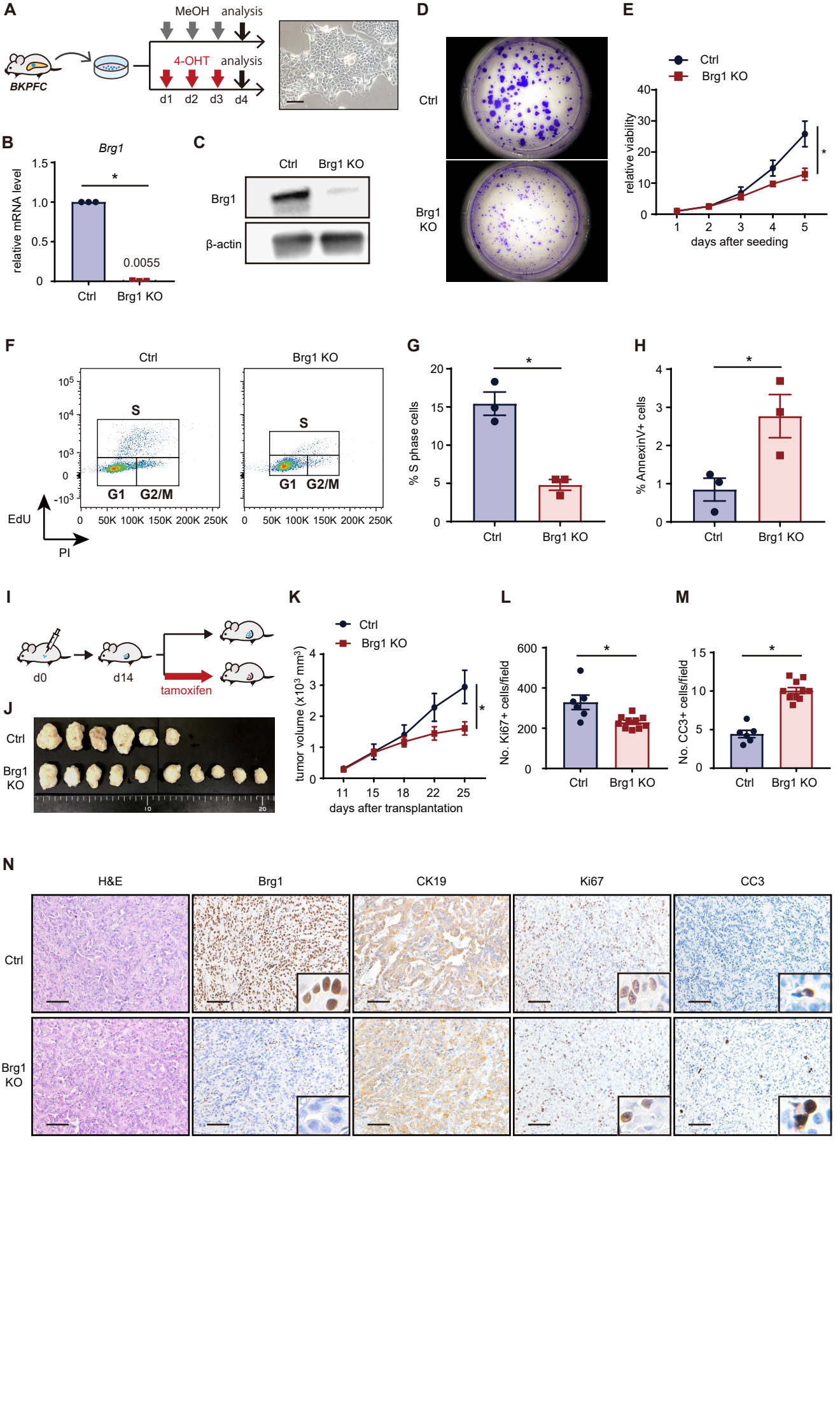
A
MeOH
analysis
4-OHT
analysis
d1
d2
d3
d4
BKPFC
B
Brg1
relative mRNA level
0.0055
Ctrl
Brg1 KO
C
Ctrl
Brg1 KO
Brg1
β-actin
D
Ctrl
Brg1 KO
E
Ctrl
Brg1 KO
relative viability
days after seeding
F
Ctrl
Brg1 KO
S
G1
G2/M
EdU
PI
G
% S phase cells
H
% AnnexinV+ cells
I
d0
d14
tamoxifen
J
Ctrl
Brg1 KO
K
Ctrl
Brg1 KO
tumor volume (x10³ mm³)
days after transplantation
L
No. Ki67+ cells/field
M
No. CC3+ cells/field
N
H&E
Brg1
CK19
Ki67
CC3
Ctrl
Brg1 KO

Figure 3

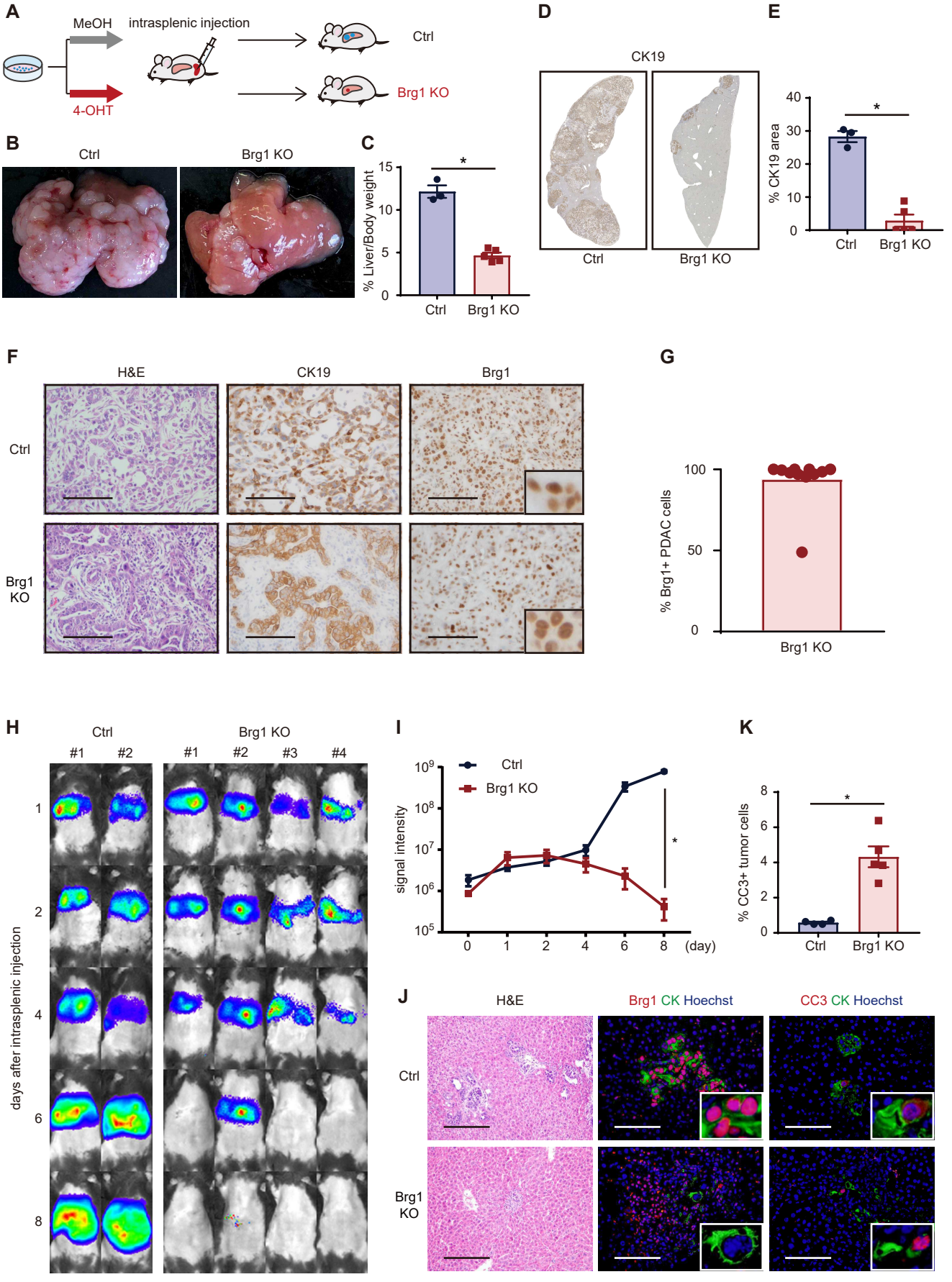
A
MeOH
intrasplenic injection
4-OHT
Ctrl
Brg1 KO
B
Ctrl
Brg1 KO
C
% Liver/Body weight
15
10
5
0
*
Ctrl
Brg1 KO
D
CK19
Ctrl
Brg1 KO
E
% CK19 area
40
30
20
10
0
*
Ctrl
Brg1 KO
F
H&E
CK19
Brg1
Ctrl
Brg1 KO
G
% Brg1+ PDAC cells
100
50
0
Brg1 KO
H
Ctrl
Brg1 KO
#1
#2
#1
#2
#3
#4
1
2
4
6
8
days after intrasplenic injection
I
signal intensity
10^9
10^8
10^7
10^6
10^5
Ctrl
Brg1 KO
*
0
1
2
4
6
8
(day)
K
% CC3+ tumor cells
8
6
4
2
0
*
Ctrl
Brg1 KO
J
H&E
Brg1 CK Hoechst
CC3 CK Hoechst
Ctrl
Brg1 KO

Figure 4

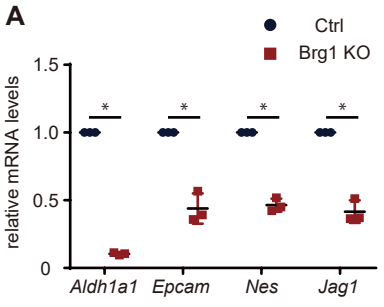

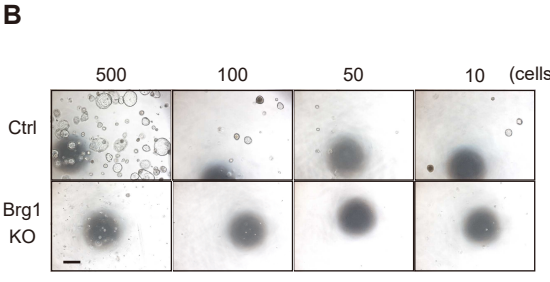

cells/well	Ctrl	Brg1 KO
500	5/5	5/5
100	5/5	3/5
50	5/5	0/5
10	3/5	0/5

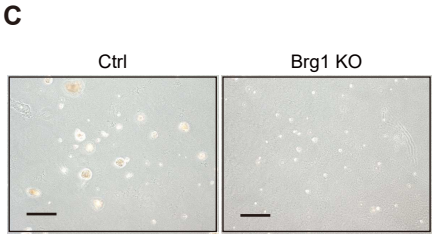

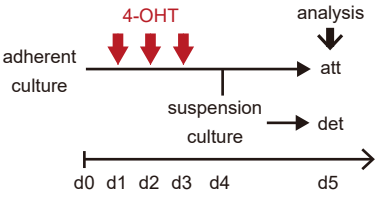

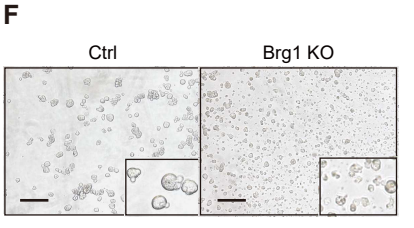

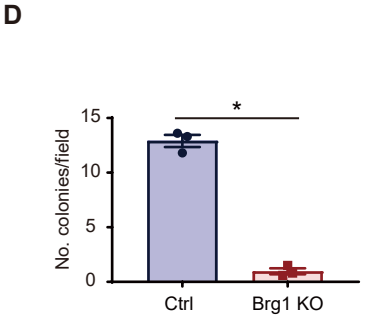

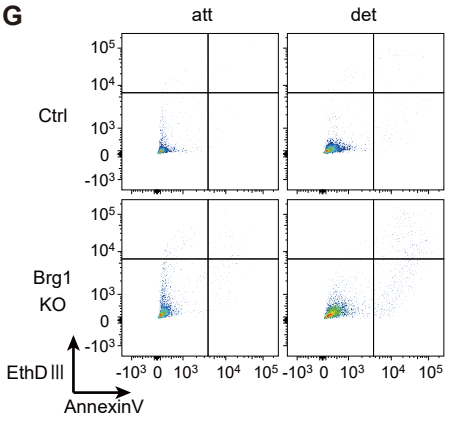

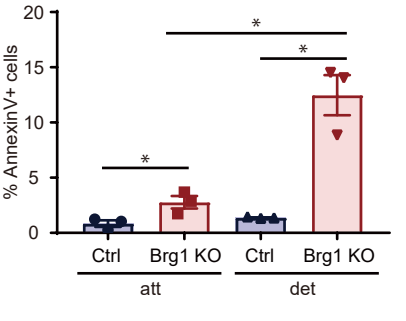

Figure 5

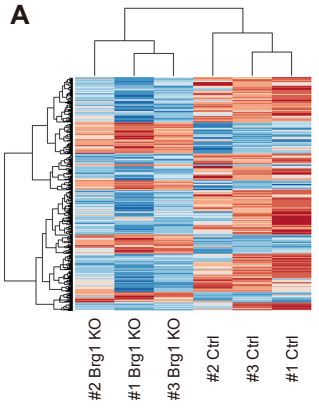

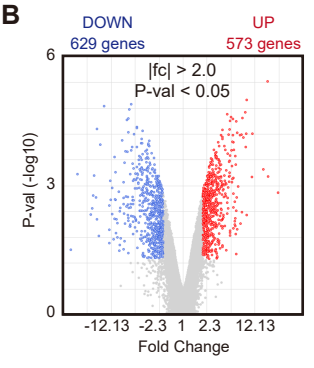

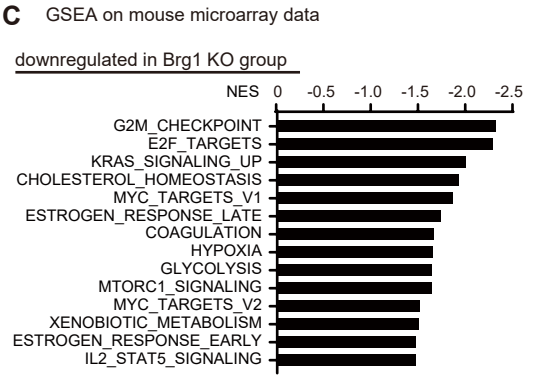

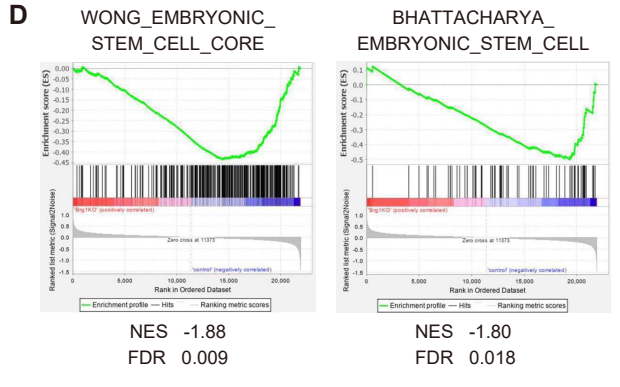

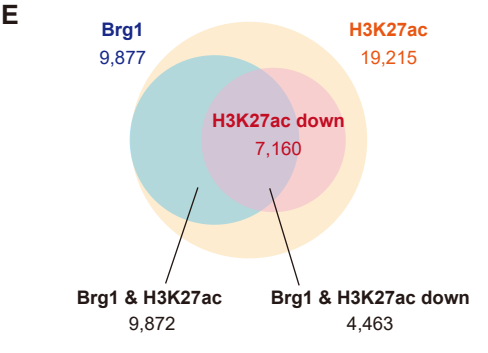

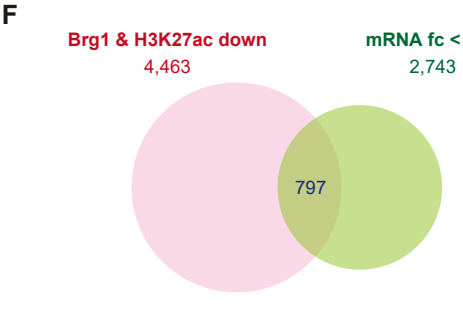

G

KEGG pathway	%	Fold Enrichment	FDR
TNF signaling pathway	2.15	3.70	0.0027
Mucin type O-Glycan biosynthesis	0.88	5.93	0.0912
HIF-1 signaling pathway	1.64	3.03	0.0912
Renal cell carcinoma	1.26	3.49	0.1020
Metabolic pathways	9.36	1.38	0.1020
Bile secretion	1.26	3.34	0.1020
Axon guidance	1.77	2.58	0.1020
Ras signaling pathway	2.53	2.07	0.1046
Rap1 signaling pathway	2.40	2.11	0.1046

Figure 6

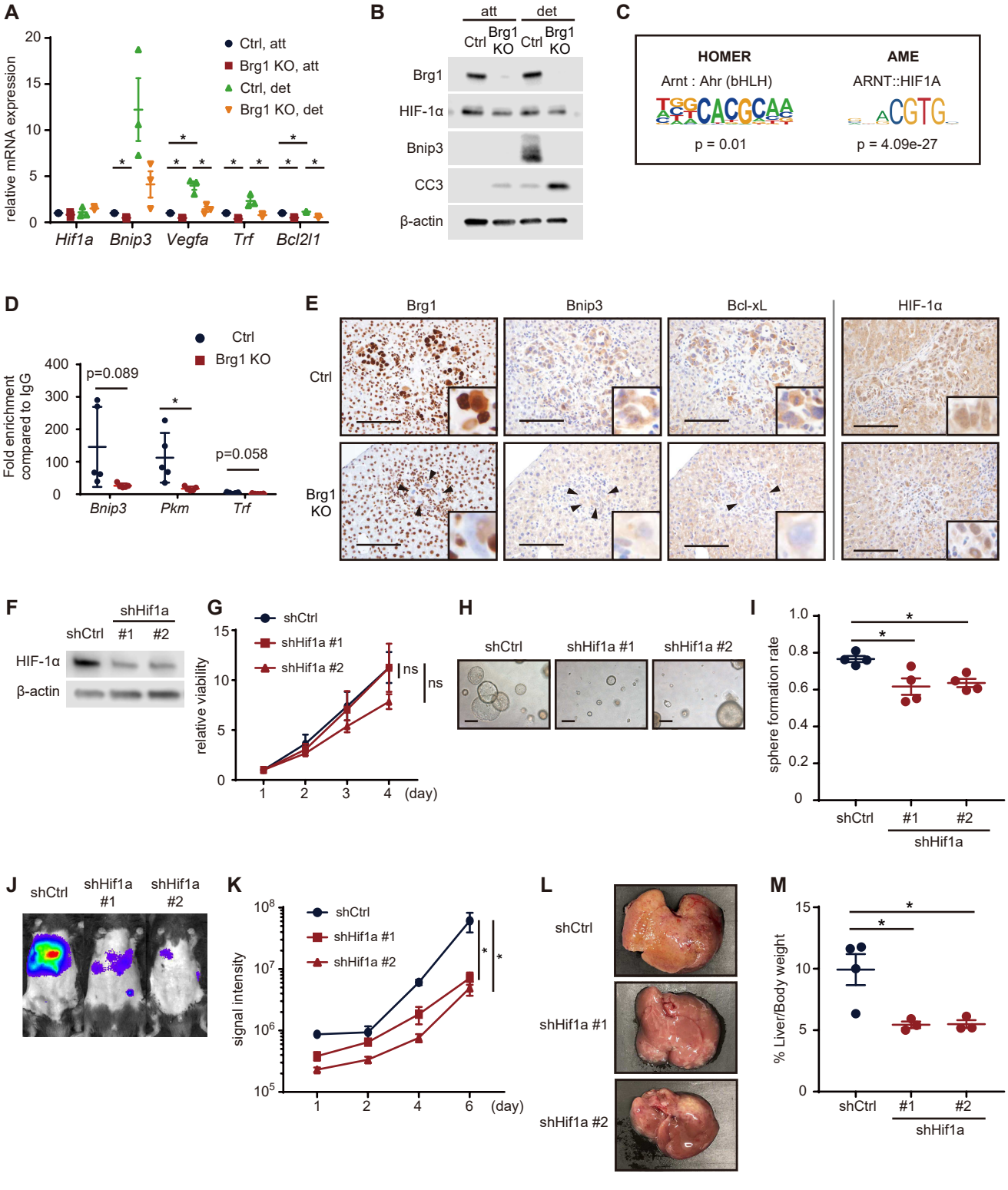
A
relative mRNA expression
Ctrl, att
Brg1 KO, att
Ctrl, det
Brg1 KO, det
Hif1a
Bnip3
Vegfa
Trf
Bcl2l1
B
att
det
Ctrl
Brg1 KO
Brg1
HIF-1α
Bnip3
CC3
β-actin
C
HOMER
Arnt : Ahr (bHLH)
p = 0.01
AME
ARNT::HIF1A
p = 4.09e-27
D
Fold enrichment compared to IgG
Ctrl
Brg1 KO
p=0.089
p=0.058
Bnip3
Pkm
Trf
E
Brg1
Bnip3
Bcl-xL
HIF-1α
Ctrl
Brg1 KO
F
shHif1a
shCtrl
#1
#2
HIF-1α
β-actin
G
shCtrl
shHif1a #1
shHif1a #2
relative viability
ns
(day)
H
shCtrl
shHif1a #1
shHif1a #2
I
sphere formation rate
shCtrl
#1
#2
shHif1a
J
shCtrl
shHif1a #1
shHif1a #2
K
shCtrl
shHif1a #1
shHif1a #2
signal intensity
(day)
L
shCtrl
shHif1a #1
shHif1a #2
M
% Liver/Body weight
shCtrl
#1
#2
shHif1a

Figure 7

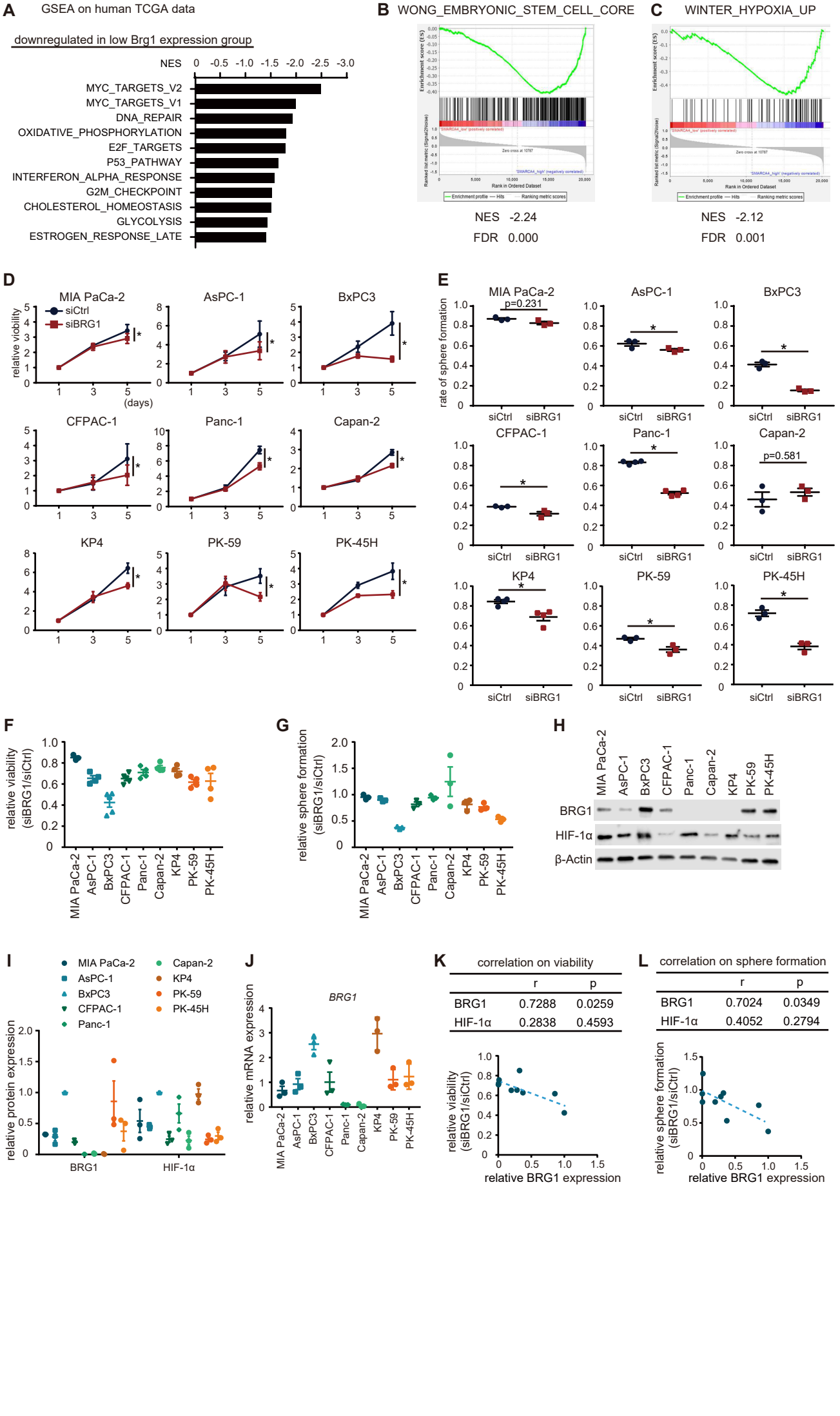
A
GSEA on human TCGA data
downregulated in low Brg1 expression group
NES 0 -0.5 -1.0 -1.5 -2.0 -2.5 -3.0
MYC_TARGETS_V2
MYC_TARGETS_V1
DNA_REPAIR
OXIDATIVE_PHOSPHORYLATION
E2F_TARGETS
P53_PATHWAY
INTERFERON_ALPHA_RESPONSE
G2M_CHECKPOINT
CHOLESTEROL_HOMEOSTASIS
GLYCOLYSIS
ESTROGEN_RESPONSE_LATE
B
WONG_EMBRYONIC_STEM_CELL_CORE
NES -2.24
FDR 0.000
C
WINTER_HYPOXIA_UP
NES -2.12
FDR 0.001
D
MIA PaCa-2
AsPC-1
BxPC3
CFPAC-1
Panc-1
Capan-2
KP4
PK-59
PK-45H
relative viability
siCtrl
siBRG1
(days)
E
rate of sphere formation
p=0.231
p=0.581
F
relative viability (siBRG1/siCtrl)
G
relative sphere formation (siBRG1/siCtrl)
H
BRG1
HIF-1α
β-Actin
I
relative protein expression
J
BRG1
relative mRNA expression
K
correlation on viability
r p
BRG1 0.7288 0.0259
HIF-1α 0.2838 0.4593
relative BRG1 expression
L
correlation on sphere formation
r p
BRG1 0.7024 0.0349
HIF-1α 0.4052 0.2794
relative BRG1 expression